IEEE Access
Multidisciplinary ⋮ Rapid Review ⋮ Open Access Journal

Received 26 August 2023, accepted 14 September 2023, date of publication 19 September 2023,
date of current version 27 September 2023.

Digital Object Identifier 10.1109/ACCESS.2023.3317171

RESEARCH ARTICLE

Fuzzy Adaptive Linear Active Disturbance Rejection Control for Quadrotor Load UAV Based on Kalman Filter

YUNPENG JU, YALIN ZHANG, AND GUIXIN ZHU
College of Automation and Electronic Engineering, Qingdao University of Science and Technology, Qingdao 266100, China
Corresponding author: Guixin Zhu (qdzgxnj@126.com)

This work was supported in part by the National Natural Science Foundation of China under Grant 61903213, and in part by the Natural Science Foundation of Shandong Province under Grant ZR2019BF039.

ABSTRACT In order to solve the problem of load variation and nonlinear strong coupling of the quadrotor load unmanned aerial vehicle (UAV), this paper proposes a fuzzy adaptive linear active disturbance rejection control algorithm based on the Kalman filter (KFFA-LADRC). Firstly, according to the established dynamics model of the quadrotor load UAV, the linear extended state observer (LESO) and the controller based on the bandwidth method are designed. Secondly, to enhance the system's adaptability and robustness, a real-time fuzzy adaptive controller is introduced to dynamically adjust the controller parameters. Furthermore, to tackle uncertainties disturbances arising from sensor noise and unknown external disturbances, the Kalman filter is utilized to predict the output state, thereby providing the optimal estimation input for the LESO. The approach not only achieves stable control of internal interference, but also reduces the dependence of the Kalman filter on the mathematical model. Finally, simulation results substantiate the efficacy of the proposed KFFA-LADRC, highlighting its robustness and adaptability when accommodating variations in load mass, sensor noise, and external interferences within unfamiliar environments.

INDEX TERMS Fuzzy adaptive, Kalman filter, linear active disturbance rejection control, quadrotor load unmanned aerial vehicle.

I. INTRODUCTION

In recent years, quadrotor unmanned aerial vehicles(UAVs) have extensively utilized across various global industries, undertaking challenging tasks such as oil pipeline patrols, high-altitude cable inspections, logistics transportation, disaster search and rescue missions [1], [2], [3], [4], [5]. Compared to fixed-wing aircraft and traditional helicopters, these UAVs offer greater flexibility and rapid responsiveness. During disaster relief efforts, a quadrotor can swiftly access isolated areas, delivering essential medical supplies, food, and communication equipment. However, during flight, they encounter challenges like sensor noise, wind disturbances, and variations in load. With six degrees of freedom and only four control inputs, they demonstrate underactuation and strong nonlinear coupling, necessitating rigorous attitude and position control.

Accompanied by technological progress, research methodologies for quadrotor UAVs have witnessed rapid advancements, particularly in the integration of adaptive control [6], [7] and reinforcement learning [8]. While adaptive control dynamically adjusts control parameters to adapt to ever-changing flight conditions, reinforcement learning determines optimal control strategies through ongoing interactions with the environment. Nevertheless, these sophisticated control methods often require higher computational resources, potentially complicating the drone's control system and increasing costs. The control landscape for quadrotors encompasses a wide array of strategies, including PID control [9], linear quadratic regulator (LQR) control [10], sliding mode control [11], LADRC control [12], neural network control [13], and H_∞ control [14],

The associate editor coordinating the review of this manuscript and approving it for publication was Mouquan Shen.

to name a few. However, each approach presents its own distinct features and constraints. For instance, LQR control relies heavily on precise dynamic models. Sliding mode control, though robust against external disturbances and parameter variations, can induce high-frequency oscillations if not properly configured. Neural networks [15], despite their speed and adaptability, may not always be suitable for systems as nonlinear and tightly coupled as quadrotors. Moreover, many control strategies tend to overlook the internal and external disturbances that quadrotors frequently encounter.

In contrast, PID control remains a popular choice due to its straightforward structure and the advantage of not relying on meticulous mathematical models. Its ease of implementation, especially on budget-friendly and energy-efficient hardware, renders it particularly suitable for quadrotor UAVs. Typically, the control framework for these UAVs employs a cascade PID strategy [16], which is bifurcated into outer and inner loops. The inner loop predominantly manages the drone's attitude via angular velocity, whereas the outer loop governs its position using angles. While the robustness and interference resistance of PID control have certain limits, its simplicity and broad applicability continue to endear it to many. Indeed, in a bid to surmount PID's inherent constraints, researchers have begun blending it with alternative control techniques. In the reference [17], it introduces an adaptive control methodology for both attitude and position in quadrotors, effectively sidestepping manual gain adjustments. Referenced [18] literature employs adaptive neural networks combined with extended Kalman filters to fine-tune PID parameters, thus diminishing control discrepancies and enhancing response times. Elsewhere, In the reference [19], a genetic algorithm tackles the optimization of linear and nonlinear constraints by adjusting PID controller parameters. In another cited study [20], incorporating both fuzzy neural networks with PID not only refines the controller's parameters and enhances the UAV's performance, but also reduces the computational demands of cascaded neural network control. Nevertheless, while these adaptations improve upon some of PID's shortcomings, the strategies deployed to counter system noise and uncertainties remain incomplete, leading to apprehensions about potential excessive error estimations and oscillations during target tracking.

To further enhance and refine the aforementioned control techniques, Professor Han Jingqing introduced the ADRC [21] approach to optimize traditional PID control. Central to this method is its ability to estimate and counteract system disturbances to meet control objectives. Notably, this technique does not rely on precise mathematical models, making it particularly suited for addressing the nonlinear, strongly coupled dynamics of quadrotor UAVs. Yet, as noted in the literature [22], the processes of sampling and discretization can degrade performance and amplify system intricacy. Discrepancies and uncertainties in system models can compromise the controller's efficacy. To address these challenges, the LADRC framework was introduced. This merges an extended state observer with an adaptive mechanism, allowing for real-time disturbance estimation, compensation, and mitigation. While LADRC offers advancements in precision and reliability compared to PID, the complexity of parameter tuning has increased. To streamline this process, references [23] utilize the bandwidth method, reducing the number of parameters and thereby broadening LADRC's applicability.

However, despite LADRC's ability to effectively estimate and counteract disturbances, improper parameter settings can lead to system instability or overshoot, particularly during load variations. To bolster the control system's adaptability and stability, fuzzy adaptive control is incorporated into LADRC. The fuzzy controller processes both the input error and its rate of change, establishing control parameters based on predefined fuzzy rules. These outputs are then defuzzified to derive the actual control parameters. This integration amplifies the system's robustness and capacity to handle non-linearities. The inclusion of the fuzzy adaptive mechanism facilitates real-time parameter estimation and tweaking, enabling the system to adeptly manage uncertainties. Reference [24] results from various studies indicate that when a controlled entity experiences internal disturbances, relying solely on PID control doesn't facilitate swift objective function tracking. However, by integrating PID with fuzzy adaptive control, the resulting fuzzy-PID demonstrates rapid tracking capabilities with enhanced robustness. In the referenced study [25], a fuzzy sliding mode controller has been crafted for longitudinal attitude decoupling, showcasing commendable adaptability. While the fuzzy controller excels in boosting system robustness and reaction times, its disturbance immunity could benefit from further refinement. Hence, integrating fuzzy control with LADRC enhances its resistance to disturbances. Building on previous work [26], a unique set of fuzzy rules has been proposed, introducing the fuzzy-LADRC methodology which boasts a quicker response and superior anti-disturbance capabilities.

In conventional LADRC designs, an extended state observer is employed to estimate the system's state and disturbances, aiming to mitigate the impact of both external and internal perturbations. However, in more intricate settings, this method may not yield the most optimal estimations. To enhance state estimation precision, the integration of the Kalman filter with LADRC is proposed. Recognized as a quintessential state estimation technique, the Kalman filter can deliver optimal state predictions when the statistical properties of system noise and disturbances are known. This filter is adept at adapting to various scenarios, optimally forecasting the entire system's state while effectively minimizing noise interference. Existing reference [27] highlights the filter's prowess in efficiently eliminating the effects of measurement and channel noise

during the control process, consequently elevating the control system's stability, responsiveness, and overall performance. Nonetheless, when internal perturbations occur within the controlled entity, the actual state deviations might not align with the system model's predictions. This misalignment can lead to significant discrepancies between the system's tracking and the preset values, causing the estimated outcomes to veer away from the system's true state. To tackle these challenges, literature [28] has introduced designs that blend the linear quadratic tracking approach and LADRC, further incorporating neural network approximators and extended Kalman filters to boost accuracy significantly. In the referenced studies [29], the Kalman filter's innate adaptability is underscored, enabling it to dynamically fine-tune estimation accuracy, thus mitigating measurement noise and enhancing the control system's overall efficiency. Collectively, these research contributions underscore the efficacy and potential of integrating the Kalman filter into LADRC methodologies.

To sum up, the main contributions of this paper are as follows:

- To address the issue of air resistance affecting the quadrotor load UAV, a mathematical model is established. Furthermore, in response to the changes in the quadrotor UAV's center of mass when the load varies, a more accurate mathematical model is designed to enhance the system's practicality.
- For quadrotor load UAVs tasked with frequent load transport, maintaining stability can pose significant challenges, especially given the internal interference from load shifts. In addressing this, the Fuzzy Adaptive LADRC (FA-LADRC) method emerges as a promising solution. Specifically designed for the stability control of quadrotor load UAVs, the FA-LADRC methodology controls both the attitude and position channels of the UAV. By integrating the robust resilience of fuzzy adaptive control with LADRC's exceptional anti-interference capabilities, this innovative system not only ensures swift and stable setpoint tracking but also proficiently mitigates disturbances arising from load alterations during transit.
- To address the impacts of sensor noise and environmental rigors on quadrotor load UAVs, a refined FA-LADRC framework augmented with the Kalman filter becomes indispensable. Positioned as a disturbance observer, when determining the observation gain w_o (LESO's observed gain) for LESO, striking the right balance between disturbance attenuation and noise impact can be challenging. This is where the Kalman filter, introduced prior to LESO, enhances the system's response speed while simultaneously reducing noise interference. Notably, their combined use dilutes the Kalman filter's reliance on strict mathematical modeling. The culmination of these interventions results in markedly improved control performance, especially in interference-ridden conditions. Furthermore, this integrated method rectifies issues associated with the Kalman filter's deviation from tracking input signals during dynamic changes in the controlled object.
- To demonstrate the feasibility of the proposed control scheme, this study conducts simulation experiments using MATLAB/SIMULINK. In the simulation experiment, PID control, without bandwidth LADRC(WB-LADRC), LADRC, FA-LADRC, and Kalman filter fuzzy adaptive LADRC(KFFA-LADRC) are introduced to compare the tracking input signals of the quadrotor load UAV. During the flight of the quadrotor load UAV, load mass changes and white noise are introduced to simulate real-life interference. These control methods are designed to mitigate the effects of interference and enhance the tracking performance of the quadrotor load UAV. By designing different control methods, the results show that the KFFA-LADRC control scheme exhibits better stability and adaptability under the interference condition. The simulation results show the feasibility of KFFA-LADRC for quadrotor load UAVs.

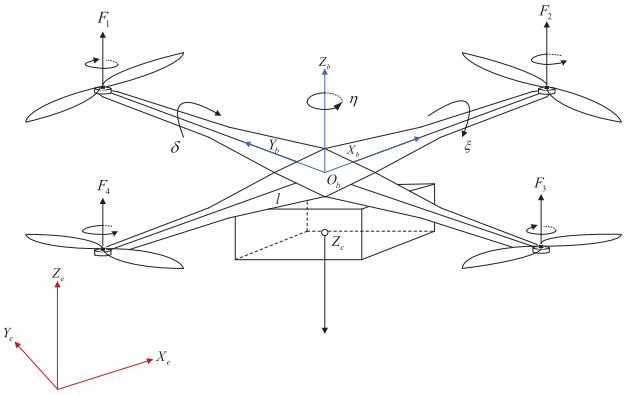

FIGURE 1. structure diagram of a quadrotor load UAV.

The structure of the remaining content of this paper is as follows: The second section describes the mathematical modeling of the quadrotor UAV; The third section outlines the design of the control scheme; In the fourth section, the simulation results and discussion of the control scheme are presented. Finally, the paper concludes with a summary.

II. DYNAMICS MODEL OF A QUADROTOR LOAD UAV

According to Fig. 1, the two adjacent rotors rotate in opposite directions to counteract the reverse moment generated by their respective rotations. The quadrotor possesses six degrees of freedom: namely x, y, and z as the position coordinates, ξ, δ, and η as the attitude coordinates, where ξ, δ, η represent roll angle, pitch angle and yaw angle.

The rotation matrix corresponding to each axis is as follows:

$$R_x(\eta) = \begin{bmatrix} 1 & 0 & 0 \\ 0 & \cos\eta & -\sin\eta \\ 0 & \sin\eta & \cos\eta \end{bmatrix},$$

$$R_y(\eta) = \begin{bmatrix} \cos\eta & 0 & \sin\eta \\ 0 & 1 & 0 \\ -\sin\eta & 0 & \cos\eta \end{bmatrix},$$
$$R_z(\eta) = \begin{bmatrix} \cos\eta & -\sin\eta & 0 \\ \sin\eta & \cos\eta & 0 \\ 0 & 0 & 1 \end{bmatrix}. \quad (1)$$

The following formula can describe the relationship between the earth-fixed frame E and the body-fixed frame B according to matrix transformation [30].

$$R = R_x(\xi) R_y(\delta) R_z(\eta) = \begin{bmatrix} M_1 & M_2 & M_3 \end{bmatrix}, \quad (2)$$

where

$$M_1 = \begin{bmatrix} \cos\delta\cos\eta \\ \cos\delta\sin\eta \\ -\sin\delta \end{bmatrix},$$
$$M_2 = \begin{bmatrix} \sin\xi\sin\delta\cos\eta - \cos\xi\sin\eta \\ \sin\xi\sin\delta\sin\eta + \cos\xi\cos\eta \\ \sin\xi\cos\delta \end{bmatrix},$$
$$M_3 = \begin{bmatrix} \cos\xi\sin\delta\cos\eta + \sin\xi\sin\eta \\ \cos\xi\sin\delta\sin\eta - \sin\xi\cos\eta \\ \cos\xi\cos\delta \end{bmatrix}. \quad (3)$$

A. POSITION DYNAMICS MODEL

According to Newton's second law, the position dynamics model of the quadrotor UAV, under the influence of various forces, can be established as follows:

$$\begin{cases} F = ma, \\ F = f + G_M + G_m + K_{f1} \\ = \left(\sum_{i=1}^{4} F_i\right) b_z + G_M + G_m + K_{f1}, \end{cases} \quad (4)$$

where F represents the combined external force acting on the quadrotor UAV, α_i denotes the total lift force of the motor, M is the mass of the quadrotor, m is the mass of the load, F_i indicates the lift provided by a single motor. The lift of the rotor is directly proportional to the square of the rotational speed, meaning the force of each motor can defined as $F_i = K_t\alpha_i^2$, where K_t is the lift coefficient of the rotor coefficient. Additionally, $G_M = \begin{bmatrix} 0 & 0 & -Mg \end{bmatrix}^T$, $G_m = \begin{bmatrix} 0 & 0 & -mg \end{bmatrix}^T$, where g denotes the acceleration due to gravity, The air resistance matrix is given by $K_{f1} = \begin{bmatrix} -K_f\dot{x} & -K_f\dot{y} & -K_f\dot{z} \end{bmatrix}^T$, with K_f being the air resistance coefficient. Applying the transformation matrix R, the following expression is obtained:

$$b_z = \begin{bmatrix} i & j & k \end{bmatrix} \begin{bmatrix} \cos\xi\sin\delta\cos\eta + \sin\xi\sin\eta \\ \cos\xi\sin\delta\sin\eta - \sin\xi\cos\eta \\ \cos\xi\cos\delta \end{bmatrix}. \quad (5)$$

According to formula (4), the following relation can be derived:

$$\left(\sum_{i=1}^{4} F_i\right) b_z + G_M + G_m + K_{f1}$$
$$= \left(\sum_{i=1}^{4} F_i\right) \begin{bmatrix} i & j & k \end{bmatrix} \begin{bmatrix} \cos\xi\sin\delta\cos\eta + \sin\xi\sin\eta \\ \cos\xi\sin\delta\sin\eta - \sin\xi\cos\eta \\ \cos\xi\cos\delta \end{bmatrix}$$
$$+ \begin{bmatrix} 0 \\ 0 \\ -Mg \end{bmatrix} + \begin{bmatrix} 0 \\ 0 \\ -mg \end{bmatrix} + \begin{bmatrix} -K_f\dot{x} \\ -K_f\dot{y} \\ -K_f\dot{z} \end{bmatrix}$$
$$= (M+m) \begin{bmatrix} i & j & k \end{bmatrix} \begin{bmatrix} \ddot{x} \\ \ddot{y} \\ \ddot{z} \end{bmatrix}. \quad (6)$$

Rearranging the above equation yields the following expression:

$$\begin{cases} \ddot{x} = \dfrac{\sum_{i=1}^{4} K_t\alpha_i^2(\cos\xi\sin\delta\cos\eta + \sin\xi\sin\eta) - K_f\dot{x}}{M+m}, \\ \ddot{y} = \dfrac{\sum_{i=1}^{4} K_t\alpha_i^2(\cos\xi\sin\delta\cos\eta + \sin\xi\sin\eta) - K_f\dot{y}}{M+m}, \\ \ddot{z} = \dfrac{\sum_{i=1}^{4} K_t\alpha_i^2(\cos\xi\cos\delta - K_f\dot{z})}{M+m} - g. \end{cases} \quad (7)$$

B. ATTITUDE DYNAMICS MODEL

The angular momentum theorem of the motion of the center of mass can be derived as:

$$M_b = \frac{dL}{dt}, \quad (8)$$

In the body coordinate system, the following expression can be obtained,

$$M_b = \frac{dL}{dt}|_b + \alpha L + K_{f2} = M_1 + M_2 + K_{f2}, \quad (9)$$

where L represents the moment of momentum, M_b denotes the combined external moment of the quadrotor UAV, M_1 is the moment generated by the lift force, M_2 is the moment generated due to the air resistance by the spiral rotor, and $K_{f_2} = \begin{bmatrix} -K_f\dot{\xi} & -K_f\dot{\delta} & -K_f\dot{\eta} \end{bmatrix}^T$ is the air resistance matrix. The lift of the rotor is directly proportional to the square of the rotational speed, so the resistance moment of each rotor $M_{2i} = K_d\nu_i^2$, where K_d is the resistance moment coefficient and ν_i is the corresponding motor speed.

$$\begin{cases} M_1 = \sum_{i=1}^{4} r_iF_i = l(F_3 - F_1) b_y + l(F_2 - F_4) b_x, \\ M_2 = K_d\left(\nu_1^2 + \nu_2^2 + \nu_3^2 + \nu_4^2\right) b_z, \\ K_{f_2} = \begin{bmatrix} -lK_f\dot{\xi} & -lK_f\dot{\delta} & -K_f\dot{\eta} \end{bmatrix}^T, \end{cases} \quad (10)$$

Combine M_1, M_2, and K_{f_2} as presented in equation (10) to obtain the following formula

$$M_b = M_1 + M_2 + K_{f_2}$$

$$= \begin{bmatrix} b_x & b_y & b_z \end{bmatrix} \begin{bmatrix} l\left(F_2 - F_4\right) - lK_f\dot{\xi} \\ l\left(F_3 - F_1\right) - lK_f\dot{\delta} \\ K_d\left(v_1^2 - v_2^2 + v_3^2 - v_4^2\right) - K_f\dot{\eta} \end{bmatrix}, \tag{11}$$

where l denotes the distance from the center of mass to the center of the motor, b_x, b_y, and b_z represent unit vectors along the x, y, and z axes respectively, r_i refers to the vector of each rotor lever, F_i is the vector corresponding to the lift force of each rotor.

$$\begin{cases} \ddot{\xi} = \dfrac{l(F_2 - F_4) - (I_z - I_y)\dot{\delta}\dot{\eta} - lK_f\dot{\xi}}{I_x}, \\ \ddot{\delta} = \dfrac{l(F_3 - F_1) - (I_x - I_z)\dot{\xi}\dot{\eta} - lK_f\dot{\delta}}{I_y}, \\ \ddot{\eta} = \dfrac{K_d(v_1^2 - v_2^2 + v_3^2 - v_4^2) - (I_y - I_x)\dot{\xi}\dot{\delta} - lK_f\dot{\eta}}{I_z}, \end{cases} \tag{12}$$

where I_x, I_y, and I_z represent the moment of inertia on the x, y, and z axes respectively.

C. DYNAMICS MODEL OF QUADROTOR LOAD UAV

When the quadrotor UAV is loaded, due to the increase in weight, the center of mass of the quadrotor load UAV moves down, and the distance from the motor to the center of mass is increased, which affects the pitch angle movement and the roll angle movement of the quadrotor UAV. The centroid coordinates of the quadrotor UAV are set as (x_1, y_1, z_1), and the centroid coordinates of the load are set as (x_2, y_2, z_2). Once connected to the payload, the quadrotor drone and its load function as a single entity. Consequently, the centroid coordinates of the quadrotor UAV after being connected to the load are as follows:

$$\begin{cases} x_a = (Mx_1 + mx_2)/(M + m), \\ y_a = (My_1 + my_2)/(M + m), \\ z_a = (Mz_1 + mz_2)/(M + m). \end{cases} \tag{13}$$

As illustrated in Fig. 1, the centroid coordinates of the quadrotor UAV are denoted by $(0, 0, 0)$, while the centroid coordinates of the load are given by $(0, 0, z_2)$. By utilizing equation (13), can calculate the coordinates labeled as $z_a = mz_2/(M + m)$. Consequently, the center of mass coordinate of the quadrotor load UAV is $(0, 0, z_a)$.

In line with the quadrotor and torque model, a virtual controlling force denoted by $U = \begin{bmatrix} U_1 & U_2 & U_3 & U_4 \end{bmatrix}^T$ is introduced, replacing the total lift force and the torque experienced at each attitude angle.

$$U = \begin{bmatrix} U_1 \\ U_2 \\ U_3 \\ U_4 \end{bmatrix} = \begin{bmatrix} f \\ M_x \\ M_y \\ M_z \end{bmatrix} = \begin{bmatrix} F_1 + F_2 + F_3 + F_4 \\ F_2 - F_4 \\ F_3 - F_1 \\ F_1 - F_2 + F_3 - F_4 \end{bmatrix}$$

TABLE 1. Units for magnetic properties.

Symbol	Description	Value
M	kg	10
m_{max}	kg	6.73
g	m/s^2	9.8
l	m	0.44
I_x	$kg \cdot m^2$	$2.906e^{-1}$
I_y	$kg \cdot m^2$	$2.906e^{-1}$
I_z	$kg \cdot m^2$	$2.906e^{-1}$
K_f	Ns^2/rad	0.15

m_{max} represents the maximum load mass of the quadrotor load UAV.

$$= \begin{bmatrix} K_t \sum_{i=1}^{4} v_i^2 \\ K_t\left(v_2^2 - v_4^2\right) \\ K_t\left(v_3^2 - v_1^2\right) \\ K_d\left(v_1^2 - v_2^2 + v_3^2 - v_4^2\right) \end{bmatrix}, \tag{14}$$

where U_1, U_2, U_3, and U_4 represent z-axis speed control input, roll-axis speed control input, pitch-axis speed control input, and yaw-axis speed control input, f is the total lift force of the quadrotor load UAV, M_x, M_y, and M_z are the rolling moment, pitching moment and yawing moment under the attitude angle respectively. According to (7), (12), (13), (14) the following formula can be obtained

$$\begin{cases} \ddot{x} = U_1\left(\cos\xi\sin\delta\cos\eta + \sin\xi\sin\eta\right)/\left(M + m\right) \\ \qquad -K_f\dot{x}/\left(M + m\right), \\ \ddot{y} = U_1\left(\cos\xi\sin\delta\sin\eta - \sin\xi\cos\eta\right)/\left(M + m\right) \\ \qquad -K_f\dot{y}/\left(M + m\right), \\ \ddot{z} = U_1(\cos\xi\cos\delta)/\left(M + m\right) - K_f\dot{z}/\left(M + m\right) - g, \\ \ddot{\xi} = U_2 l/I_x + \left(I_z - I_y\right)\dot{\delta}\dot{\eta}/I_x - lK_f\dot{\xi}/I_x, \\ \ddot{\delta} = U_3 l/I_y + \left(I_x - I_z\right)\dot{\xi}\dot{\eta}/I_y - lK_f\dot{\delta}/I_y, \\ \ddot{\eta} = U_4/I_z + \left(I_y - I_x\right)\dot{\xi}\dot{\delta}/I_z - K_f\dot{\eta}/I_z, \\ l = \sqrt[2]{{l_0}^2 + {z_a}^2}, \end{cases} \tag{15}$$

where l_0 represents the distance from the origin of the quadrotor load UAV coordinate system to the center.

In the simulation experiment, the parameters utilized for the quadrotor UAV are detailed in Table 1:

III. DESIGN OF KALMAN FUZZY ADAPTIVE LINEAR ACTIVE DISTURBANCE REJECTION CONTROL

The quadrotor load UAV operates using four motors, adjusting their speeds to dictate its movement. As depicted in Fig. 2, both the attitude and position rings of the UAV are under the governance of the KFFA-LADRC system, where FAC represents the fuzzy adaptive control, and KF stands for the Kalman filter. The operational procedure begins by inputting a signal into the LADRC. As the system endeavors to track the objective function, any arising discrepancies or errors are channeled into the fuzzy control as inputs. Post fuzzy logic processing, the controller's bandwidth is ascertained and then applied back to the LADRC, ensuring

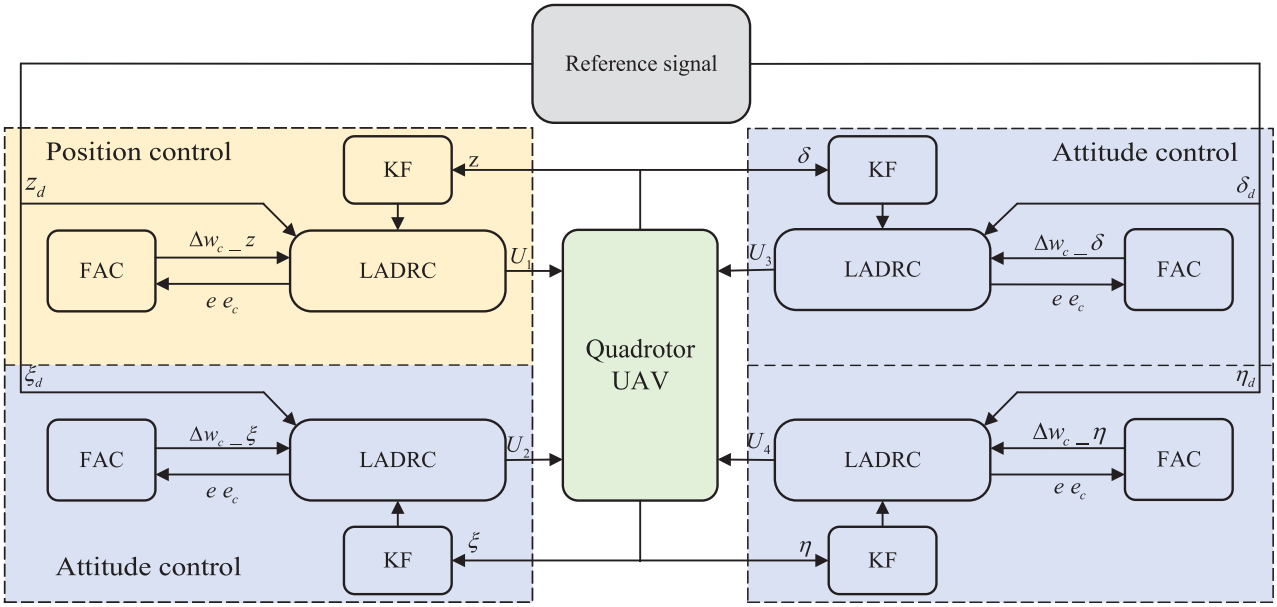

FIGURE 2. Block diagram of control scheme.

the system retains agility while bolstering its robustness. Subsequent to this, the LADRC computes the control amount, and treats it as an input for the object being regulated, aiming to closely adhere the input value. Recognizing the need to enhance the system's performance and minimize noise, a Kalman filter is incorporated. This filter refines the tracking values prior to them being routed to the LESO. The incorporation of this step amplifies the system's observational and estimation prowess. Collectively, these processes form an integrated closed-loop control system, designed to maximize accuracy and efficiency.

A. DESIGN OF LINEAR ACTIVE DISTURBANCE REJECTION CONTROL

The LADRC generates differential signals for the entire control system using a tracking differentiator (TD) and orchestrates the transition process. The LESO employed in the control scheme exhibits fast response and robust anti-interference capabilities. Both internal and external disturbances are regarded as the total disturbance of the system, and can be compensated for by the linear control rate. For instance, in the case of height control, the controller is shown in Fig. 3.

1) DESIGN OF TRACKING DIFFERENTIATOR

When the setpoint is entered into the control system, the large system response caused by the step signal can be mitigated by introducing a transition process, to achieve smooth setpoint tracking and improve the stability of the control system.

According to the theory of optimal control, the discrete system is the optimal control function, referred to as *fhan*,

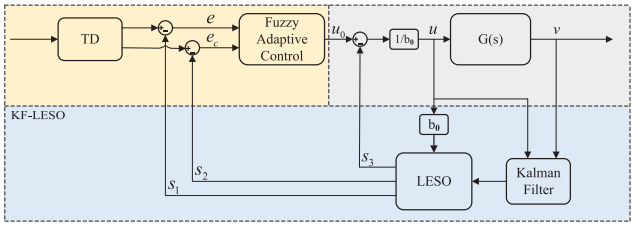

FIGURE 3. Structure diagram of controller.

which can be defined as follows:

$$\begin{cases} q = ih^2, \\ c_0 = hc_2, \\ c_1 = \sqrt{q(q + 8\,|y|)}, \\ c_2 = c_0 + sign(y)(c_1 - q)/2, \\ fsg(x, q) = (sign(x + q) - sign(x - q))/2, \\ c_0 = (c_0 + y)fsg(y, q) + c_2(1 - fsg(y, q)), \\ fhan = -r(c/q)fsg(c, q) - rsign(c)(1 - fsg(c, q)), \end{cases} \tag{16}$$

Based on equation (16), further arrangements can be made for the transition process.

$$\begin{cases} fh = fhan(x_a(k) - v(k), x_b(k), i, h_0), \\ x_a(k + 1) = x_a(k) + hx_b(k), \\ x_b(k + 1) = x_b(k) + hfh, \end{cases} \tag{17}$$

where h represents the simulation time step, h_0 denotes the smoothing factor, and i indicates the velocity factor. As the velocity factor increases, the transition takes less time, but i reaches a point where the transition is so fast that

the tracking signal overshoots or oscillates. In the control simulation experiment the values are assigned as follows: $h = 0.005, h_0 = 0.1, i = 200$.

2) DESIGN OF LINEAR EXTENDED STATE OBSERVER

Based on the TD, the LESO is introduced to enhance the LADRC system. Consider a class of nonlinear time-varying systems with singular input-single output:

$$v^{(n)}(t) = f\left(v^{(n-1)}(t), \cdots, v(t), w(t)\right) + bu \tag{18}$$

where u and v are the input and output of the controlled object system, respectively, b is the control gain coefficient, and $w(t)$ is the external disturbance, $v^{(n)}(t) = f\left(v^{(n-1)}(t), \cdots, v(t), w(t)\right)$ indicates that the controlled object is dynamic, which can be linear time-varying system, and can be represented by f, where let $v^{(k)} = p_{k+1}, k = 1, 2, \ldots, n-1$, and let $p_{n+1} = f$. Therefore, the dynamic characteristics of the system can be articulated as follows:

$$\begin{cases} \dot{p}_1 = p_2, \\ \vdots \\ \dot{p}_{n-1} = p_n, \\ \dot{p}_n = p_{n+1} + bu, \\ v = p_1, \end{cases} \tag{19}$$

where p_{n+1} is the extended state, which provides an accurate estimate of the internal state of the system by observing all the state-changing effects of the system except for the control inputs. The LESO is constructed according to (19).

$$\begin{cases} \dot{\hat{s}}_1 = \hat{s}_2 + l_1(p_1 - \hat{s}_1), \\ \vdots \\ \dot{\hat{s}}_{n-1} = \hat{s}_n + l_{n-1}(p_1 - \hat{s}_1), \\ \dot{\hat{s}}_n = \hat{s}_{n+1} + l_n(p_1 - \hat{s}_1) + bu, \\ \dot{\hat{s}}_{n+1} = l_{n+1}(p_1 - \hat{s}_1), \end{cases} \tag{20}$$

where $\hat{S} = \left[\hat{s}_1\ \hat{s}_2 \cdots \hat{s}_{n+1}\right]^T \in R^{n+1}, l_i, i = 1, 2, \ldots, n+1$ is the gain parameters of the LESO, which exhibits minimal dependence on the system model. Instead, it is primarily associated with the order of the controlled object. Consequently, the dynamic height channel of the quadrotor load UAV can be derived from equation (15).

$$\begin{cases} \dot{p}_1 = p_2 \\ \dot{p}_2 = u(\cos\xi\cos\delta)/(M+m) + f_0 \\ f_0 = -K_f\dot{z}/(M+m) - g \\ y = p_1 \end{cases} \tag{21}$$

where $P = [p_1, p_2]^T$ is a measurable state of a second-order system, u is the system input, and f is the state in the formula other than the system input, called the total disturbance of the LADRC system.

Define $s_1 = p$, $s_2 = \hat{p}$, and $s_3 = f$ as representations of LESO. For the second-order controlled object, in order to accurately estimate the two state variables and the disturbance signal of the system, it is necessary to select a higher bandwidth than the order of the controlled object. Therefore, a third-order observer is designed, where $S = \left[s_1\ s_2\ s_3\right]^T$, the nonlinear system is derived according to equation (20).

$$\begin{cases} \dot{S} = AS + Bu + Eh \\ V = CS \end{cases} \tag{22}$$

where $A = \begin{bmatrix} 0 & 1 & 0 \\ 0 & 0 & 1 \\ 0 & 0 & 0 \end{bmatrix}$, $B = \left[0\ b\ 0\right]^T$,
$E = \left[0\ 0\ 1\right]^T$, $C = \left[1\ 0\ 0\right]$.
The LESO is

$$\begin{cases} \dot{\hat{p}} = A\hat{p} + Bu + L(v - \hat{v}), \\ \hat{v} = C\hat{p}, \end{cases} \tag{23}$$

where $L = \left[l_1\ l_2\ l_3\right]^T$ is the vector of LESO gain in a linear active disturbance rejection controller.

3) DESIGN OF THE LINEAR CONTROL RATE

Based on the TD and LESO methods, the control rates can be designed according to the system's requirements and performance standards as follows:

$$u = (u_0 - \hat{s}_3)/b_0, \tag{24}$$

where u is the output of the PD controller, b_0 is the controller constant, its function is to compensate for the static error in the system.

$$u_0 = k_p\left(r - \hat{s}_1\right) + k_d\left(\dot{r} - \hat{s}_2\right) \tag{25}$$

where r represents the input signal, k_p denotes the proportional coefficient of the LADRC controller, and k_d is the differential coefficient.

4) PARAMETER TUNING

Building upon the foundations of the LESO and PD controller, this paper introduces a bandwidth reference [31] to optimize the LADRC system. This approach not only ensures system stability but also diminishes the number of parameters within the control system. The bandwidth method is serves to allocate the pole of the characteristic equation. By positioning the pole of the control loop is located in the left half-plane, the system maintains continual stability.

$$[s_a - (-w)]^n = s_a^{n+1} + w\alpha_1 s_a^n + \cdots + w^n\alpha_n s_a + w^{n+1}\alpha_{n+1}, \tag{26}$$

where

$$\left[l_1\ l_2\ \cdots l_{n+1}\right] = \left[w\alpha_1\ w^2\alpha_2 \cdots w^{n+1}\alpha_{n+1},\right] \tag{27}$$

where $w > 0$, and $\alpha_i, i = 1, 2\cdots, n+1$ is the coefficients of the characteristic polynomial.

$L = \left[3w_o\ 3w_o^2\ w_o^3\right]$ can be obtained from (22), (26), where w_o is the bandwidth of LESO.

$k_p = w_c^2$,$k_d = 2w_c$ can be obtained from (25), (26), where w_c is the bandwidth of the PD controller.

(1) Controller parameters w_c

The approximate closed-loop transfer function of the controller system of equation (25) can be obtained as

$$\hat{G}_{cl}(s) = \frac{w_c^2}{(s+w_c)^2}. \tag{28}$$

Formula (28) corresponds to the unit step signal

$$Y(s) = \frac{w_c^2}{(s+w_c)^2}\frac{1}{s} = \frac{1}{s} - \frac{1}{s+w_c} - \frac{w_c}{(s+w_c)^2}. \tag{29}$$

The inverse Laplace transform of the formula (29) is obtained

$$y(t) = 1 - (1 + w_c t_s)\, e^{-w_c t}, \tag{30}$$

As illustrated by the aforementioned formula, $y(t)$ escalates monotonically without any overshoot. It is apparent that the adjustment time t_s is predominantly influenced by the parameter w_c. Consequently, the crucial task in tuning the bandwidth of the PD controller lies in selecting an appropriate value for w_c to achieve a satisfactory adjustment time for the system.

$$|y(t_s - y(\infty))| = (1 + w_c t_s)\, e^{-w_c t_s} \le \Delta\%, \tag{31}$$

The adjustment time t_s can be obtained by solving the following transcendental equation

$$(1 + w_c t_s)\, e^{-w_c t_s} = \Delta\%, \tag{32}$$

It is obtained by numerical method

$$\begin{cases} t_s = 4.74/w_c, \Delta = 2, \\ t_s = 5.83/w_c, \Delta = 5. \end{cases} \tag{33}$$

Select $\Delta = 2$ and keep a certain margin, which can be made in the actual design.

Choose an appropriate adjustment time t_s while retaining a certain margin, thereby facilitating the actual design of the following relationship:

$$t_s = \frac{(8-10)}{w_c}. \tag{34}$$

In the PD controller, the bandwidth w_c of the PD controller can be obtained through the calculation of the formula (34). The gain of the noise transfer function increases with the increase of the high-frequency band as the bandwidth w_c. Therefore, it is necessary to balance the system's noise immunity and response time when choosing w_c.

(2) LESO parameters w_o

In the LESO system, the gain w_o serves a critical role in shaping the system's performance. As illustrated in the referenced [32] article, it is directly proportional to the control gain, represented by the equation $w_o = cw_c$. In essence, elevating the observer gain can diminish the system's overshoot. However, this action also results in a slower system response. Moreover, adjusting this gain noticeably enhances the system's sensitivity to its parameter settings. Consequently, the constant c is typically adjusted within the range of 5 to 10,

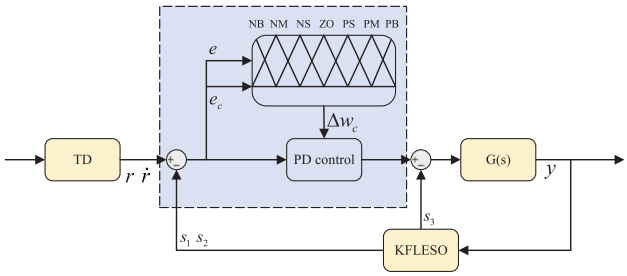

FIGURE 4. Structure diagram of fuzzy control.

$$w_o = (5-10)\, w_c. \tag{35}$$

(3) Control quantity coefficient b_0

Selecting an optimal value for b_0 facilitates achieving a desired steady-state output devoid of disturbances. As illustrated in equation (15), the optimal selection for the compensation gain can be expressed as $b_0 = (\cos\xi\cos\delta)/(M+m)$. However, due to the strong coupling characteristics of the quadrotor load UAV, the value of b_0 changes in real-time. Therefore, the design value of b_0 is as follows:

$$\begin{cases} \ddot{z} = b_0 u + f, \\ f = [\cos\xi\cos\delta/(M+m) - b_0]u - K_f \dot{z}/(M+m) - g. \end{cases} \tag{36}$$

According to $\cos\xi\cos\delta/(M+m) \le \cos\xi\cos\delta/M \le 1/M$, let

$$b_0 = 1/M \tag{37}$$

B. DESIGN OF THE FUZZY ADAPTIVE CONTROL

Quadrotor load UAVs, when executing missions, frequently adjust to varying loads, causing their mathematical models to change often. Relying on fixed controller parameters in such dynamic environments is not always optimal. To address this, this paper integrates fuzzy control technology into the LADRC control system. This fuzzy controller transitions continuous values into fuzzy values, processed via a set of predefined fuzzy rules. Afterward, these fuzzy values undergo defuzzification, transforming them back into continuous control signals. Working alongside the LADRC controller, the parameters are dynamically tailored using fuzzy logic. As the quadrotor manages different loads, the system experiences these variations as internal disturbances. The crux of fuzzy adaptive control lies in discerning the fuzzy relationship among the PD controller's bandwidth w_c, error e, and error rate e_c. By doing so, the control parameters can be dynamically adjusted. In the reference [33], should the system encounter external interferences, the fuzzy controller steps in, generating suitable control signals that promptly counteract these interferences, ensuring system stability. This

approach offers the dual advantage of rapid target tracking and diminished noise in the LESO post stabilization. In real-world application, the fuzzy controller employs the sensitive triangular membership function to monitor e and e_c in real-time. This allows for the dynamic adjustment of w_c based on fuzzy control rules, enhancing the system's adaptability. To provide a visual understanding, the Z-axis channel's fuzzy adaptive controller structure is depicted in Fig. 4.

Seven fuzzy sets have been designed for the input x_1 and x_2 of the fuzzy system, that is, if $n = 2, i = 1, 2, p_1 = p_2 = 7$, then there are $p_1 \times p_2 = 49$ fuzzy rules. The fuzzy system is constructed in the following two steps.

Step 1: For variable $x_i\,(i = 1, 2)$, define p_i fuzzy sets $A_i^{l_i}\,(l_i = 1, 2, \cdots 7)$.

Step 2: $\prod_{i=1}^{n} p_i = p_1 \times p_2 = 49$ fuzzy rules are used to construct the fuzzy system, then the fuzzy rule j is

$$R^{(j)} : IF\ x_1\ is\ A_1^{l_1}\ and\ x_2\ is\ A_1^{l_2}\ THEN\ \hat{f}\ is\ B^{l_1 l_2}, \tag{38}$$

where $l_i = 1, 2, \cdots, 7, i = 1, 2, j = 1, 2, \cdots 49$, $B^{l_1 l_2}$ is the fuzzy set of the conclusion. Fuzzy rules 1 and 49 are denoted as

$$\begin{aligned} &R^{(1)} : IF\ x_1\ is\ A_1^1\ and\ x_2\ is\ A_2^1\ THEN\ \hat{f}\ is\ B^1, \\ &\vdots \\ &R^{(49)} : IF\ x_1\ is\ A_1^7\ and\ x_2\ is\ A_2^7\ THEN\ \hat{f}\ is\ B^{49}. \end{aligned} \tag{39}$$

The fuzzy reasoning process adopts the following four steps:

(1) The product inference machine is utilized to carry out the premise inference of the rule, yielding the inference result $\prod_{i=1}^{2} \mu_{A_i^{l_i}}(x_i)$.

(2) The single-value fuzzer is employed to find $\bar{y}_f^{l_1 l_2}$, which represents the function value $f(x_1, x_2)$ corresponding to the maximum value (1.0) of the membership function at the horizontal coordinates (x_1, x_2).

(3) The product inference machine is used to realize the principle of rule premise and rule conclusion, and the inference result is $\bar{y}_f^{l_1 l_2}\left(\prod_{i=1}^{2} \mu_{A_i^{l_i}}(x_i)\right)$; When all the fuzzy rules are combined, the output of the fuzzy system is $\sum_{l_1=1}^{7}\sum_{l_2=1}^{7} \bar{y}_f^{l_1 l_2}\left(\prod_{i=1}^{2} \mu_{A_i^{l_i}}(x_i)\right)$.

(4) Utilizing the average defuzzer, the fuzzy system yields the following output:

$$\hat{f}(x) = \frac{\sum_{l_1=1}^{7}\sum_{l_2=1}^{7} \bar{y}_f^{l_1 l_2}\left(\prod_{i=1}^{2} \mu_{A_i^{l_i}}(x_i)\right)}{\sum_{l_1=1}^{7}\sum_{l_2=1}^{7}\left(\prod_{i=1}^{2} \mu_{A_i^{l_i}}(x_i)\right)}, \tag{40}$$

where $\mu_{A_i^{l_i}}(x_i)$ represents the membership function of x_i.

Let $\bar{y}_f^{l_1 l_2}$ be a free parameter, placed in the set $\theta \in R^{(49)}$. By incorporating the fuzzy basis vector $\beta(x)$, equation 40 transforms as follows:

$$\hat{f}(x) = \hat{\theta}^T \beta(x), \tag{41}$$

where $\beta(x)$ is the base vector of a $\prod_{i=1}^{n} p_i = p_1 \times p_2 = 49$ dimensional fuzzy vector, whose $l_1\ l_2$ element is

$$\beta(x) = \frac{\prod_{i=1}^{2} \mu_{A_i^{l_i}}(x_i)}{\sum_{l_1=1}^{7}\sum_{l_2=1}^{7}\left(\prod_{i=1}^{2} \mu_{A_i^{l_i}}(x_i)\right)}. \tag{42}$$

To quickly track the value of the objective function and maintain sensitivity to minute errors, the parameters' characteristics define their range of variation. This range serves as the basic discourse domain for the fuzzy set represented by $e, \dot{e}, \Delta w_c = (-4, -3, -2, -1, 0, 1, 2, 3, 4)$. The fuzzy control's input and output both consist of seven linguistic variables, namely: Negative Large (NB), Negative Medium (NM), Negative Small (NS), Zero (ZO), Positive Small (PS), Positive Medium (PM), and Positive Large (PB). The fuzzy rules for w_c are detailed in Table 2.

Firstly, the appropriate system parameter $\hat{w}_c$ is found according to equation (31), then fuzzy rules are formulated according to parameter characteristics, and finally, the revised value Δw_c is obtained by the weighted average method, such that $w_c = \hat{w}_c + \Delta w_c$.

TABLE 2. Units for magnetic properties.

w_c		e_c						
		NB	NM	NS	ZO	PS	PM	PM
e	NB	PB	PB	PB	PB	PS	ZO	ZO
	NM	PB	PB	PM	PM	PS	ZO	ZO
	NS	PM	PM	PS	PS	ZO	ZO	NS
	ZO	PM	PS	PS	ZO	NS	NS	NM
	PS	PS	ZO	ZO	NS	NM	NM	NM
	PM	ZO	ZO	NS	NM	NM	NB	NB
	PB	ZO	NS	NM	NM	NB	NB	NB

C. DESIGN OF THE KALMAN FILTER

According to formula (21), discretizing the linear system results in the following formula,

$$\begin{cases} p_{(k)} = Ap_{(k-1)} + B(u_{(k-1)} + w_{(k)}), \\ y_{v(k)} = Cp_{(k)} + v_{(k)}, \end{cases} \tag{43}$$

where $p_{(k-1)}$ represents the system state vector, $u_{(k-1)}$ denotes the input control vector, $w_{(k)}$ indicates the process noise and $v_{(k)}$ is the measurement noise, A is the state transition matrix, which describes how to predict the state at time k from the state at time $k-1$, B is the control matrix, which describes how the control input $u_{(k)}$ and process noise $w_{(k)}$ affect the state of the system, and C is the output matrix, which describes how the state of the system is transformed into the observed output.

The combination of LESO and Kalman filter is shown in Fig. 5.

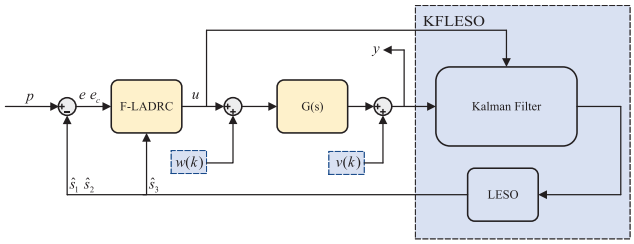

FIGURE 5. Structure diagram of Kalman fuzzy adaptive linear active disturbance rejection control.

The LESO employs a Kalman filter to enhance its estimation capabilities. By comparing the measured values with the predicted values from the model, the Kalman filter refines the system state estimation, thereby improving measurement accuracy. LESO, serving as a disturbance observer, diligently assesses and counterbalances the system's unknown disturbances, ensuring formidable resistance against such unforeseen perturbations. While a heightened observation gain, w_o, is beneficial for disturbance suppression, it can inadvertently influence the bandwidth in channels susceptible to noise. To balance the dual challenges of reducing disturbance and managing noise, the Kalman filter steps in. It amplifies the bandwidth, thereby elevating both the system's response agility and its suppression prowess. The Kalman filter, beyond its bandwidth enhancement role, offers a superior starting point for LESO's state estimations, rooted in both the model and measurements. Concurrently, it effectively reduces measurement noise, fortifying the overall robustness and stability of the control framework.

In the realm of Kalman filtering, integrating LESO reduces the reliance on pinpoint accurate mathematical models. Within the LADRC framework, LESO is tasked with gauging and counterbalancing the system's internal disturbances. It primarily considers the compensation gain and the input data of the entity being controlled. Notably, LESO's cumulative disturbance is akin to the process noise, $w_{(k)}$, in the Kalman filter. Even when confronted with shifting system dynamics or incomplete models, LESO stands resilient, adeptly offsetting unmodeled disturbances and errors. This finesse streamlines the Kalman filter's operational model, circumventing undue intricacies. Under the LADRC umbrella, the Kalman filter's principal role pivots around rectifying biases in LESO's estimates and compensations. This refines the system's state estimations, ensuring they remain both precise and robust. Consequently, it further diminishes the necessity for impeccably accurate mathematical models.

The Kalman filter can be divided into two processes: Prediction and correction. The prediction is to establish a prior estimate of the current state using the time update equation, and to construct a prior estimate of the next state according to the previous calculation. The correction is to establish an improved posterior estimate of the current state on the basis of the prior estimate, and uses the current measurement variable to obtain the optimal estimate using the measurement update equation. This iterative process is known as the estimation-correction process, and the corresponding estimation algorithm is called the prediction-correction algorithm. Within the recursive Kalman filter design, the notation $\bar{}$ represents the prior estimate, while $\hat{}$ represents the optimal estimate. The recursive Kalman filter design is as follows:

Kalman filters use previous state estimates and covariance matrices to make predictions about the output data,

$$\hat{p}_{(k)}^{-} = F\hat{p}_{(k-1)} + G\hat{U}_{(k-1)}, \tag{44}$$

The error variance is predicted from the dynamic model of the system and previous state estimates

$$E_{(k)}^{-} = FE_{(k-1)}F^T + Q, \tag{45}$$

The Kalman gain is calculated by comparing the prediction error variance with the observed noise

$$N_{m(k)} = E_{(k)}^{-}H^T\left(HE_{(k)}^{-}H^T + R\right)^{-1}, \tag{46}$$

By using the predicted state and measured data, the optimal estimation of system state output is obtained by Kalman gain weighting

$$\hat{p}_{(k)} = \hat{p}_{(k)}^{-} + N_{m(k)}\left(W_{v(k)} - H\hat{p}_{(k)}^{-}\right), \tag{47}$$

By calculating the Kalman gain, the filter can modify the error variance of the previous state estimation to improve the accuracy of the estimation

$$E_{(k)} = \left(I - N_{m(k)}H\right)E_{(k)}^{-} \quad , \tag{48}$$

where F is the $n \times n$ state change matrix acting on $\hat{p}_{(k-1)}$, G is the $n \times n$ state change matrix acting on $\hat{U}_{(k-1)}$, H is $m \times n$ observation model matrix, namely, measurement system coefficient matrix, $E_{(k)}^{-}$ is the $n \times n$ prior estimation error covariance matrix, $E_{(k)}$ is the $n \times n$ posterior estimation error covariance matrix, N_m is a matrix of order $n \times m$, which is called Kalman gain, Q is $n \times n$ process noise covariance matrix, R is $m \times m$ process noise covariance matrix, I is $n \times n$ identity matrix.

The Kalman filter plays an important role in predicting and estimating the state of the system. Q and R as parameters in the Kalman filter, have a significant impact on the performance and reliability of the system. Q represents the variance of the system noise. A smaller value of Q results in easier system convergence and higher confidence in the model prediction. However, if the internal disturbance of the LADRC becomes too large, it may exceed the range of the Q value, causing the system to deviate from the desired tracking input signal. On the other hand, R represents the variance of the measurement noise. A larger value of R decreases confidence in newly measured values, while a smaller value of R can speed up system convergence but may introduce system oscillations. In order to solve these problems and optimize the performance of the Kalman filter, the internal

TABLE 3. Units for magnetic properties.

	w_c	w_o	b_0
Z	30	260	0.1
ξ	25	240	2
δ	25	240	2
η	25	240	2

parameters of the Kalman filter are designed based on the maximum tracking error of total disturbance compensation.

When the controlled object experiences internal disturbances, a maximum tracking error of 0.01 (representing the quadrotor UAV's heaviest load) is classified as internal noise. However, this only accounts for the system's internal disturbances. The system model may still be vulnerable to other uncertainties like unmodeled dynamics or white noise. Given this, there's a need to raise the value of Q, which is ultimately set at 0.03. In the conducted experiments, once tracking stabilized, a deviation approximating 0.03 in Gaussian white noise emerged. This deviation offers a foundational estimate for R: calculating 0.03^2 yields 0.0009. But, to cater to system robustness and account for potential unforeseen disturbances, a larger R-value is typically preferred. Based on simulations and real-world testing, an R-value range of 0.0005 to 0.0015 is advised. The optimal R value for system performance, pinpointed through this process, is 0.001. Thus, the parameters are set: $Q = 0.03$ and $R = 0.001$. Implementing these optimized values enhances the system's tracking precision, ensuring optimal performance even amidst varying interferences.

IV. SIMULATION RESULTS AND DISCUSSIONS

In this part, this paper will use MATLAB/SIMULINK for the simulation test of the system, where the initial value of the attitude angle is (0, 0, 0), the initial value of the height is 0m, and the parameters of the quadrotor load UAV are shown in Table. 1. According to (34), (35), (37), the parameters of the controller can be obtained, as shown in Table. 3.

A. EXAMPLE 1: TRACKING STEP SIGNAL

In the wake of increasingly frequent natural calamities, such as earthquakes and wildfires, there's an undeniable emphasis on elevating the speed and efficacy of rescue operations. Consequently, the ability of quadrotor load UAVs to swiftly track set values during high-speed flights becomes a pivotal factor in rescue outcomes. To validate the alacrity of our control approach, experimental simulations were conducted. For these tests, the weight of the unloaded quadrotor UAV was standardized at 10 kg. Various control methods were compared for efficacy, namely PID control, WB-LADRC, LADRC, and FA-LADRC. The system's input signal parameters were set as follows: $\xi = 0.5$, $\delta = 0.5$, $\eta = 0.5$, and $Z = 5$. Fig. 6 graphically represents the tracking trajectories for system altitude, as well as for the roll, pitch, and yaw angles. Complementing this, Fig. 7 visualizes the error trajectories for each of these channels. The comparative insights drawn from these figures illuminate the advantages and potential shortcomings of each control methodology, offering a clear roadmap for optimization.

TABLE 4. Time required to track setpoints (t/s).

	Z-channel	Roll-channel	Pitch-channel	Yaw-channel
PID	–	–	1.09	–
WB-LADRC	0.61	0.58	0.59	0.6
LADRC	0.4	0.43	0.41	0.38
FA-LADRC	0.3	0.29	0.3	0.29

"–" indicates that the control method has not reached stability before 1.2s

In the data outlined in Table 4, a comparative analysis reveals distinct performance metrics for each control strategy:

- The PID control, while managing to stabilize the yaw angle within 1.2 seconds, failed to achieve similar results for other channels within this time frame.
- WB-LADRC exhibits minimal overshoot, yet it demands approximately 0.6 seconds to stabilize its tracking – a duration that could be deemed suboptimal in critical scenarios.
- LADRC showcases a notable performance, settling into a steady state in about 0.4 seconds without any overshoot, marking it as a favorable approach in quick stabilization contexts.
- The FA-LADRC that stands out remarkably. It takes a mere 0.3 seconds to achieve stable tracking, outperforming all other tested methods both in terms of rapidity and stability.

This analysis underscores the superiority of FA-LADRC in scenarios demanding quick and stable responses, making it a top contender for applications where time is of the essence.

Through the analysis of the tracking error e, it is evident that both PID and WB-LADRC exhibit sluggishness in achieving stable tracking due to overshoot. In contrast, the LADRC and FA-LADRC approaches, employing the bandwidth method, effectively track the input signals without encountering overshoot in both the altitude and attitude channels. Furthermore, these channels demonstrate that FA-LADRC yields superior performance with smaller errors compared to other control methods. These findings underscore the ability of FA-LADRC to more rapidly and reliably bring the system to the desired set value.

The simulation results show that FA-LADRC is superior to other controls. FA-LADRC has the advantages of no overshoot and faster response speed, and can track input signals quickly and stably. Absolutely, the empirical outcomes solidify the proficiency of the FA-LADRC control technique presented in this study. Its capability to swiftly and accurately navigate to a designated point underscores its potential in scenarios like reconnaissance or expedited delivery of critical supplies. This emphasizes its importance in time-sensitive situations, particularly in emergency or disaster response contexts.

B. EXAMPLE 2: TRACKING TRIANGLE WAVE SIGNAL

The utilization of the triangular wave signal as the input signal in this experiment phase offers a dynamic and more

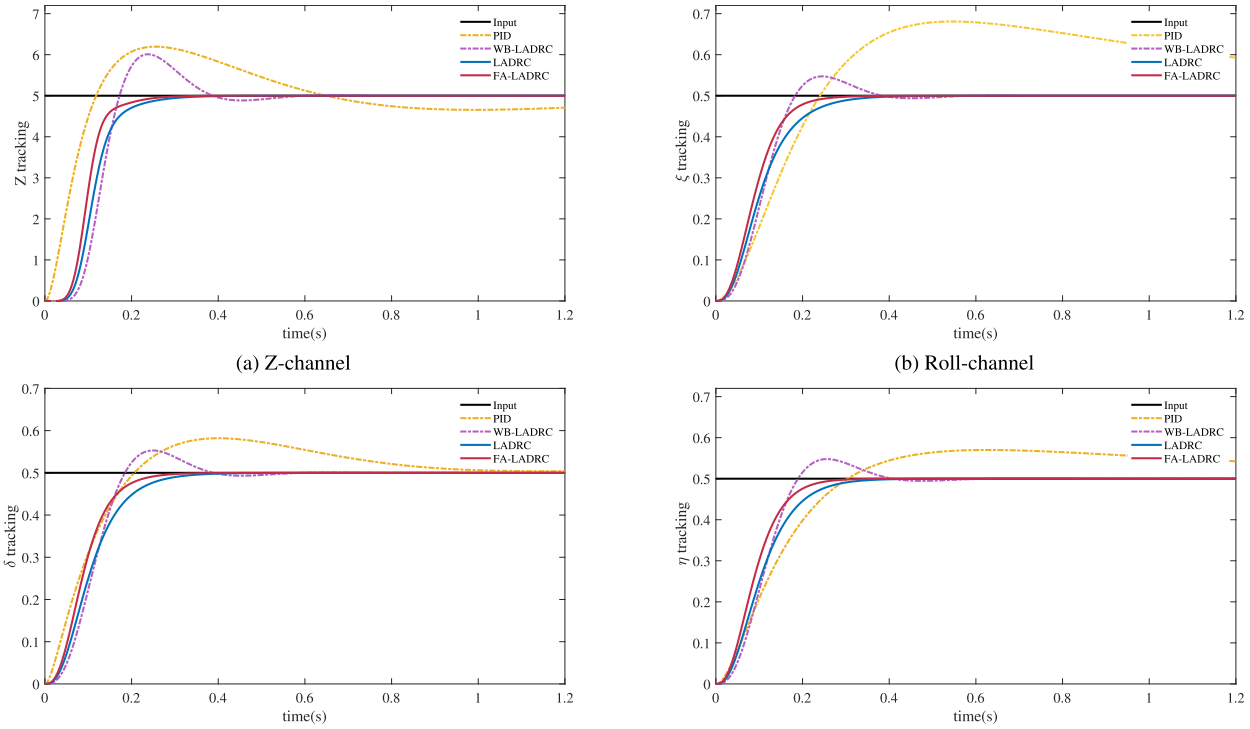

(a) Z-channel (b) Roll-channel

(c) Pitch-channel (d) Yaw-channel

FIGURE 6. The results of tracking step signal.

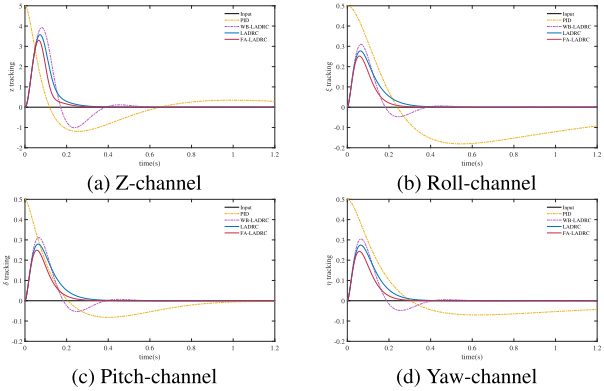

(a) Z-channel (b) Roll-channel

(c) Pitch-channel (d) Yaw-channel

FIGURE 7. Comparison of error *e* in tracking step signal experiment.

complex test scenario, mirroring real-world fluctuations and unpredictabilities that a quadrotor load UAV might encounter, especially during high-stress situations like earthquake relief. The altitude channel, reflecting the UAV's vertical movement, serves as an indicator of its ability to ascend or descend smoothly, which is crucial when navigating through uneven terrains or obstacles typically found in disaster-stricken areas. The rolling channel's lateral movement performance provides insights into the UAV's potential to sidestep obstructions or change direction promptly. Similarly, the pitch channel's forward movement, while simultaneously climbing or descending, tests the UAV's dexterity in potentially tight spaces. Finally, the yaw angle channel's tracking of the UAV's heading rotation measures its ability to efficiently reorient its direction – an essential feature during surveys or search and rescue operations. The comparative tracking simulation results displayed in Fig. 8 between PID control, WB-LADRC, LADRC, and FA-LADRC provide a comprehensive insight into each control strategy's performance under these demanding and varied conditions. The ultimate goal is to discern which method offers the best combination of agility and stability, making it the most suitable for real-world earthquake relief missions.

From the simulation results shown in Fig. 8, it is observed that the PID control exhibits poor tracking performance in the altitude channel and attitude angle channel. The input signal is not reliably tracked before descending, indicating instability in the control scheme. On the other hand, WB-LADRC, LADRC, and FA-LADRC exhibit a slight delay of 0.1 seconds in tracking the triangular wave, but they demonstrate effective tracking and rapid convergence to the set point with each change in the triangular wave. In these channels, LADRC and FA-LADRC outperform WB-LADRC in terms of responsiveness, without experiencing any overshoot. Particularly in the altitude channel, FA-LADRC remains stable even when the quadrotor UAV undergoes changes in its motion state, resulting in superior control performance.

In summary, the results in Fig. 8 demonstrate that the FA-LADRC control method has a better tracking effect on

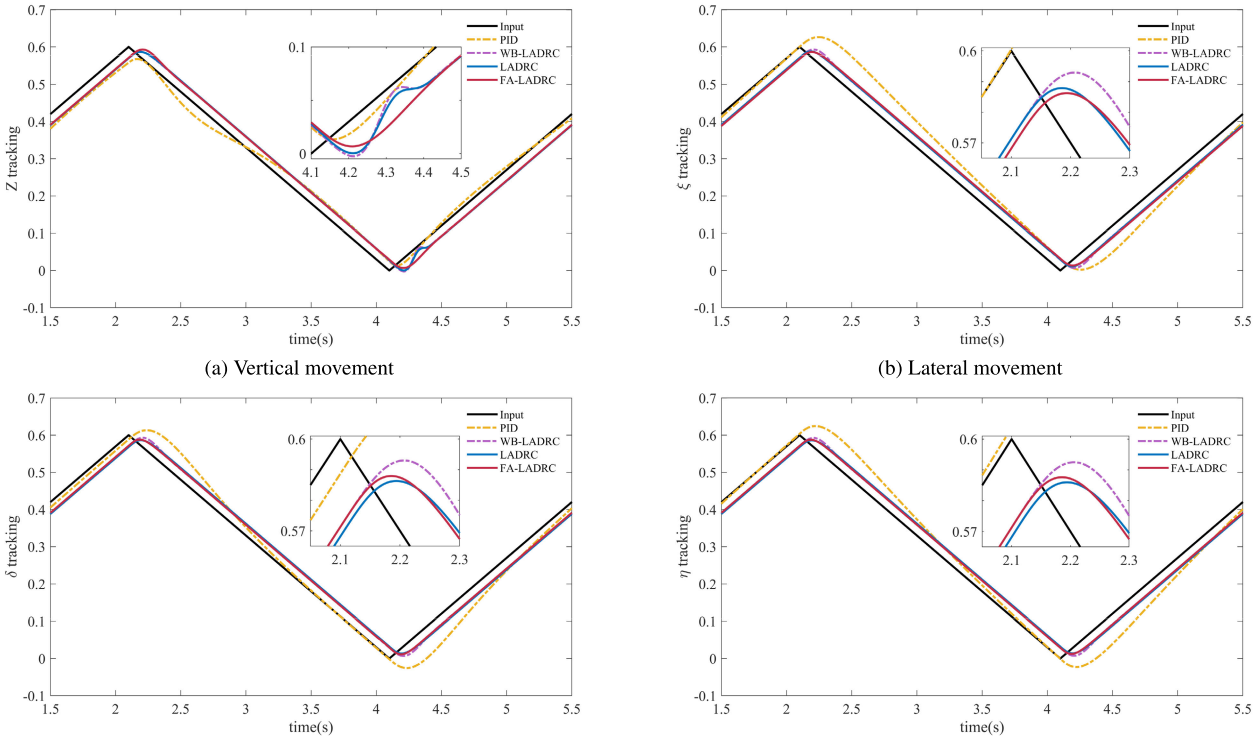

(a) Vertical movement

(b) Lateral movement

(c) Forward simultaneously ascending or descending

(d) Rotating heading

FIGURE 8. The results of tracking triangle wave signal.

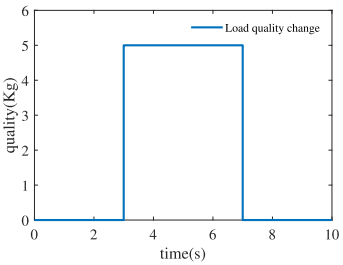

FIGURE 9. Load variation of a quadrotor load UAV.

triangular waves than other control methods, so the FA-LADRC control scheme is also effective for time-varying signals (such as triangular wave signals).

C. EXAMPLE 3: LOAD CHANGE

In disaster relief efforts following earthquakes, quadrotor load UAVs serve a dual purpose. They swiftly scout and evaluate the affected areas using high-definition cameras and facilitate the delivery of vital supplies to regions that are challenging to access. This study delves into understanding the ramifications of changes in the load on the quadrotor UAV. Fig. 9 graphically presents these load dynamics: it starts unburdened, takes on a 5 kg load at the 3-second mark, and sheds this weight at the 7-second point. Notably, throughout this simulation, the UAV's internal system parameters remain constant, treating the fluctuating weight as an external variable. For this experiment, three control mechanisms–PID control, FA-LADRC, and KFFA-LADRC–are benchmarked. Their performance outcomes are captured in Fig. 10. Furthermore, given that load-induced changes cause shifts in the k_p and k_d parameters of both the FA-LADRC and KFFA-LADRC, we have spotlighted the height and roll angle channels for a deeper dive. Their simulated responses under these conditions are depicted in Fig. 11 and Fig. 12, respectively.

Based on the results of Fig. 10, the following conclusions can be drawn: The disturbance influence of KFFA-LADRC is also less than that of FA-LADRC, and in the case that both are adaptive tuning controllers, the output tracking of the set value in FA-LADRC with the Kalman filter is more stable, which can quickly return to the set value, thus making the system more stable. In contrast, PID control is more affected by internal disturbance changes, resulting in system instability.

In FA-LADRC and KFFA-LADRC, due to the internal disturbance caused by the change of load quality, the fuzzy adaptive mechanism adjusts k_p and k_d parameters in real-time according to the mutation of the controlled object tracking input signal, so as to realize the stable and fast tracking of the input signal of the system. KFFA-LADRC optimizes the internal disturbance as the total disturbance to make the controller more stable.

Through an examination of the simulation outcomes, we can deduce that the adaptive design of FA-LADRC

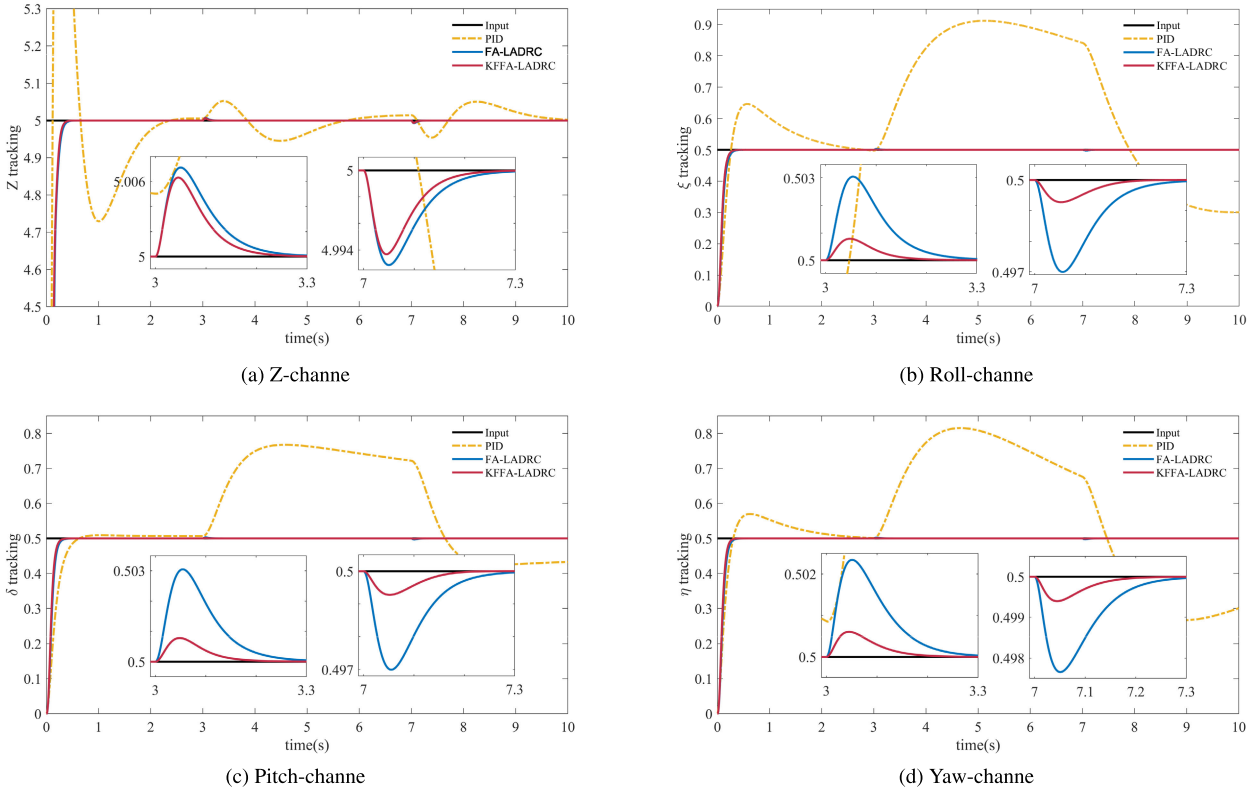

(a) Z-channe (b) Roll-channe

(c) Pitch-channe (d) Yaw-channe

FIGURE 10. The result of load variation of a quadrotor Load UAV.

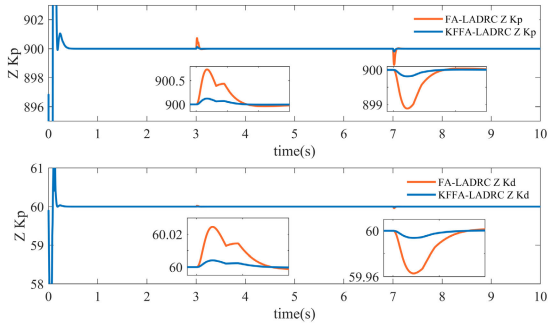

FIGURE 11. The result ofchange in K_p and K_d of Z-channel during load changes.

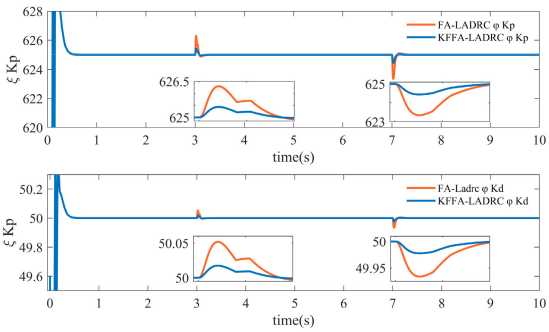

FIGURE 12. The result ofchange in K_p and K_d of Roll-channel during load changes.

is potent, curbing the impact of load mass variations on a quadrotor bearing weight. Incorporating the Kalman filter adds another layer of stability to the control system. These findings not only lay a solid foundation for the practical deployment of KFFA-LADRC but also underscore its potential. They highlight that when the quadrotor load UAV is in transit or executing material deliveries, it maintains controlled stability, thereby amplifying the efficacy of rescue operations.

D. EXAMPLE 4: DISTURBANCE EXPERIMENT

During emergency responses to natural disasters, the unpredictable and intricate environmental conditions intensify the stability and swift response requirements for rescue equipment, with drones being particularly crucial. To emulate the resilience of UAVs amidst such challenging scenarios, our experiment integrates Gaussian white noise, representing the stability control dynamics of quadrotor UAVs in severe conditions.

This simulation acknowledges multiple internal disturbances potentially impacting a quadrotor UAV. These encompass noise from the Inertial Measurement Unit (IMU), disturbances linked to the motor, and propulsion systems. Given this backdrop, we've chosen a Gaussian white noise model characterized by a mean value of 0 and a standard deviation of 0.03 to represent these internal disruptions.

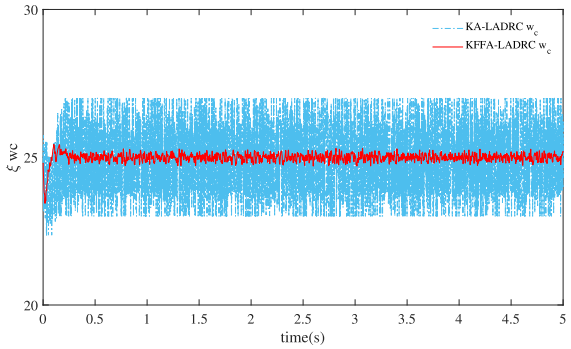

(a) The controller bandwidth w_c value changes in the environment 1

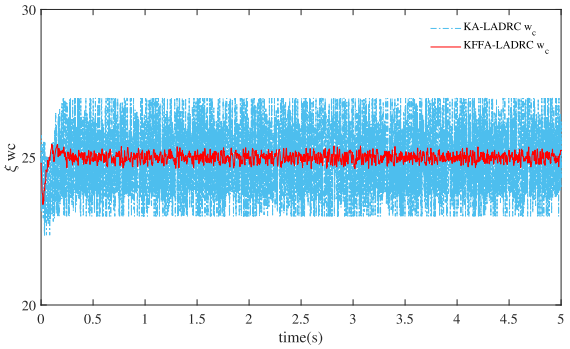

(b) The controller bandwidth w_c value changes in the environment 2

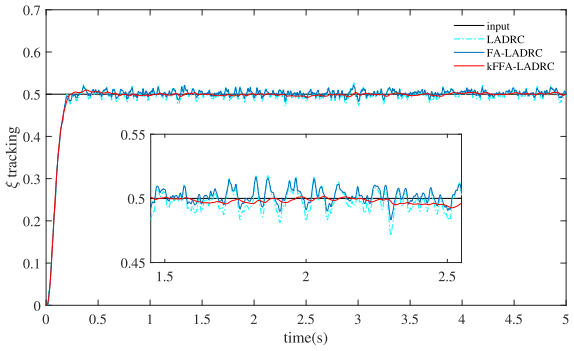

(c) Roll-channel in the environment 1

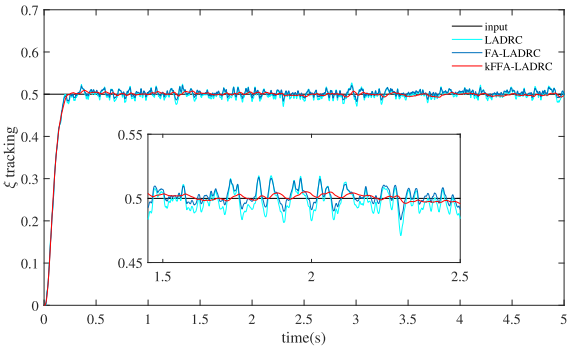

(d) Roll-channel in the environment 2

FIGURE 13. **Experimental results of disturbance.**

Springboarding from this noise model, we've conceptualized two stringent environmental simulations:

(1) An examination of the quadrotor UAV's behavior during load fluctuations.

(2) A representation where the UAV encounters interference from a vertically oriented sine-wave airflow, described as $d_z = 2sin(t)$.

In our analysis, we've primarily zeroed in on the roll angle channel, though similar patterns were observed in other channels. We've implemented two control methodologies: FA-LADRC and KFFA-LADRC. Fig. 13(a) and Fig. 13(c) portray the variations in the controller parameter w_c and the system's adeptness at aligning with preset values in the inaugural simulation. In parallel, Fig. 13(b) and Fig. 13(d) provide insights into the controller parameter shifts and the system's proficiency at honing in on setpoints within the latter simulation framework.

To prove the effectiveness of KFFA-LADRC, through the analysis of Fig. 13(a) and Fig. 13(b), it can be observed that the parameter w_c in the fuzzy adaptive controller is adjusted in real time, it dynamically adjusts the controller parameters according to the system state, and can eliminate the deviation and improve the control accuracy. This shows that the fuzzy adaptive controller is effective in the case of adding white noise. Furthermore, upon comparing the simulation results in Fig. 13(a) and Fig. 13(b), the FA-LADRC with Kalman filter, in which the parameter w_c of the controller fluctuates less, thus making the controller more stable. This shows that the control system with the Kalman filter is effective.

From Fig. 13(c) and Fig. 13(d), it's evident that the input signal for fuzzy adaptive tracking is more diminutive than that of the LADRC. Furthermore, the integration of the Kalman filter considerably diminishes the error in the tracking input signal. This ensures enhanced system stability across diverse environments.

From the aforementioned simulation results, it's clear that the KFFA-LADRC control method is highly effective. This approach not only bolsters the system's resistance to interference but also enhances the stability of the fuzzy adaptive controller. The experiment underscores the pivotal role of the control method for quadrotor load UAVs in disaster relief efforts. Thanks to its superior maneuverability and resilience to interference, it furnishes rescue teams with invaluable real-time intelligence in a range of sudden and unpredictable scenarios. This, in turn, amplifies the efficacy and safety of rescue missions.

V. CONCLUSION

This research study focuses on addressing the issue of load variation in quadrotor load UAVs. A dynamic model is established, and a control method based on KFFA-LADRC is proposed to tackle this problem. The integration of fuzzy adaptive control into the system enhances the response speed and reduces the tracking time for setpoint values. Additionally, the inclusion of the Kalman filter

in combination with LADRC helps mitigate interference effects on the quadrotor load UAV, thereby improving controller accuracy and reducing reliance on the mathematical model.

The experimental results highlight the significant performance improvements achieved by the KFFA-LADRC in terms of setpoint tracking and anti-jamming capability for the quadrotor load UAV. The method enhances stability control performance, leading to advancements in application levels, safety, and economic benefits. Particularly, these enhancements are valuable for critical applications such as earthquake relief material transportation and operations in challenging environments.

In future studies, our focus will be on exploring the practical feasibility of the proposed control scheme and refining it based on the insights gained from experimental results. Additionally, we will investigate the impact of ceiling effects and ground effects on loaded quadrotor drones. We plan to explore the utilization of neural network fuzzy adaptive control methods to optimize controller parameters, aiming to achieve faster and more stable tracking effects. The ultimate objective is to identify the optimal control scheme that enhances robustness and overall performance.

The outcomes of this research possess significant scientific value and demonstrate promising prospects for practical applications. By effectively solving the control challenges of quadrotor load UAVs, this study provides strong support for the utilization of such UAVs in disaster relief operations and demanding environments. The findings of this paper contribute to advancing the field of stability control in quadrotor load UAVs, enabling stable control of these quadrotor UAVs even in critical situations.

REFERENCES

[1] P. Cao, Y. Liu, C. Yang, S. Xie, and K. Xie, "MEC-driven UAV-enabled routine inspection scheme in wind farm under wind influence," *IEEE Access*, vol. 7, pp. 179252–179265, 2019.

[2] M. Car, L. Markovic, A. Ivanovic, M. Orsag, and S. Bogdan, "Autonomous wind-turbine blade inspection using LiDAR-equipped unmanned aerial vehicle," *IEEE Access*, vol. 8, pp. 131380–131387, 2020.

[3] Z. Zhou, C. Zhang, C. Xu, F. Xiong, Y. Zhang, and T. Umer, "Energy-efficient industrial Internet of UAVs for power line inspection in smart grid," *IEEE Trans. Ind. Informat.*, vol. 14, no. 6, pp. 2705–2714, Jun. 2018.

[4] S. Kim, D. Kim, S. Jeong, J.-W. Ham, J.-K. Lee, and K.-Y. Oh, "Fault diagnosis of power transmission lines using a UAV-mounted smart inspection system," *IEEE Access*, vol. 8, pp. 149999–150009, 2020.

[5] W. Wang, "Multi-rotor UAV design and application in fire fighting and rescue operations," *Electron. Compon. Inf. Technol.*, vol. 6, pp. 185–187, Jan. 2022.

[6] Q. Han, Z. Liu, H. Su, and X. Liu, "Filter-based disturbance observer and adaptive control for Euler–Lagrange systems with application to a quadrotor UAV," *IEEE Trans. Ind. Electron.*, vol. 70, no. 8, pp. 8437–8445, Aug. 2023.

[7] I. H. Imran, R. Stolkin, and A. Montazeri, "Adaptive control of quadrotor unmanned aerial vehicle with time-varying uncertainties," *IEEE Access*, vol. 11, pp. 19710–19724, 2023.

[8] Y. Zhou, X. Ma, S. Hu, D. Zhou, N. Cheng, and N. Lu, "QoE-driven adaptive deployment strategy of multi-UAV networks based on hybrid deep reinforcement learning," *IEEE Internet Things J.*, vol. 9, no. 8, pp. 5868–5881, Apr. 2022.

[9] S. Abdelhay and A. Zakriti, "Modeling of a quadcopter trajectory tracking system using PID controller," *Proc. Manuf.*, vol. 32, pp. 564–571, Jan. 2019.

[10] M. Okasha, J. Kralev, and M. Islam, "Design and experimental comparison of PID, LQR and MPC stabilizing controllers for parrot mambo mini-drone," *Aerospace*, vol. 9, no. 6, p. 298, Jun. 2022.

[11] Z. Liu, X. Liu, J. Chen, and C. Fang, "Altitude control for variable load quadrotor via learning rate based robust sliding mode controller," *IEEE Access*, vol. 7, pp. 9736–9744, 2019.

[12] J. Wang, X. Wang, Z. Luo, and F. Assadian, "Active disturbance rejection control of differential drive assist steering for electric vehicles," *Energies*, vol. 13, no. 10, p. 2647, May 2020.

[13] X.-Z. Jin, T. He, X.-M. Wu, H. Wang, and J. Chi, "Robust adaptive neural network-based compensation control of a class of quadrotor aircrafts," *J. Franklin Inst.*, vol. 357, no. 17, pp. 12241–12263, Nov. 2020.

[14] Z. Wang, Q. Wang, and C. Dong, "Asynchronous H_∞ control for unmanned aerial vehicles: Switched polytopic system approach," *IEEE/CAA J. Autom. Sinica*, vol. 2, no. 2, pp. 207–216, Apr. 2015.

[15] W. Liu, T. Zhao, Z. Wu, and W. Huang, "Linear active disturbance rejection control for hysteresis compensation based on backpropagation neural networks adaptive control," *Trans. Inst. Meas. Control*, vol. 43, no. 4, pp. 915–924, Feb. 2021.

[16] R. Miranda-Colorado and L. T. Aguilar, "Robust PID control of quadrotors with power reduction analysis," *ISA Trans.*, vol. 98, pp. 47–62, Mar. 2020.

[17] A. Noordin, M. A. Mohd Basri, Z. Mohamed, and I. Mat Lazim, "Adaptive PID controller using sliding mode control approaches for quadrotor UAV attitude and position stabilization," *Arabian J. Sci. Eng.*, vol. 46, no. 2, pp. 963–981, Feb. 2021.

[18] C. Rosales, S. Tosetti, C. Soria, and F. Rossomando, "Neural adaptive PID control of a quadrotor using EFK," *IEEE Latin Amer. Trans.*, vol. 16, no. 11, pp. 2722–2730, Nov. 2018.

[19] C.-L. Lee and C.-C. Peng, "Analytic time domain specifications PID controller design for a class of 2^{nd} order linear systems: A genetic algorithm method," *IEEE Access*, vol. 9, pp. 99266–99275, 2021.

[20] J. Rao, B. Li, Z. Zhang, D. Chen, and W. Giernacki, "Position control of quadrotor UAV based on cascade fuzzy neural network," *Energies*, vol. 15, no. 5, p. 1763, Feb. 2022.

[21] J. Han, "From PID to active disturbance rejection control," *IEEE Trans. Ind. Electron.*, vol. 56, no. 3, pp. 900–906, Mar. 2009.

[22] J. Dou, X. Kong, and B. Wen, "Altitude and attitude active disturbance rejection controller design of a quadrotor unmanned aerial vehicle," *Proc. Inst. Mech. Eng., G, J. Aerosp. Eng.*, vol. 231, no. 9, pp. 1732–1745, Jul. 2017.

[23] R. Zhou, C. Fu, and W. Tan, "Implementation of linear controllers via active disturbance rejection control structure," *IEEE Trans. Ind. Electron.*, vol. 68, no. 7, pp. 6217–6226, Jul. 2021.

[24] Y. Liu, K. Fan, and Q. Ouyang, "Intelligent traction control method based on model predictive fuzzy PID control and online optimization for permanent magnetic maglev trains," *IEEE Access*, vol. 9, pp. 29032–29046, 2021.

[25] K. Li, Y. Wei, C. Wang, and H. Deng, "Longitudinal attitude control decoupling algorithm based on the fuzzy sliding mode of a coaxial-rotor UAV," *Electronics*, vol. 8, no. 1, p. 107, Jan. 2019.

[26] C. Sun, C. Liu, X. Feng, and X. Jiao, "Visual servoing of flying robot based on fuzzy adaptive linear active disturbance rejection control," *IEEE Trans. Circuits Syst. II, Exp. Briefs*, vol. 68, no. 7, pp. 2558–2562, Jul. 2021.

[27] X. Tang, Q. Zhang, and L. Hu, "An EKF-based performance enhancement scheme for stochastic nonlinear systems by dynamic set-point adjustment," *IEEE Access*, vol. 8, pp. 62261–62272, 2020.

[28] H. Taghavifar, C. Hu, Y. Qin, and C. Wei, "EKF-neural network observer based type-2 fuzzy control of autonomous vehicles," *IEEE Trans. Intell. Transp. Syst.*, vol. 22, no. 8, pp. 4788–4800, Aug. 2021.

[29] Z. Yang, Z. Yan, Y. Lu, W. Wang, L. Yu, and Y. Geng, "Double DOF strategy for continuous-wave pulse generator based on extended Kalman filter and adaptive linear active disturbance rejection control," *IEEE Trans. Power Electron.*, vol. 37, no. 2, pp. 1382–1393, Feb. 2022.
[30] A. Eskandarpour and I. Sharf, "A constrained error-based MPC for path following of quadrotor with stability analysis," *Nonlinear Dyn.*, vol. 99, no. 2, pp. 899–918, Jan. 2020.
[31] Q. Zheng, L. Q. Gao, and Z. Gao, "On validation of extended state observer through analysis and experimentation," *J. Dyn. Syst., Meas., Control*, vol. 134, no. 2, Mar. 2012, Art. no. 024505.
[32] Y. Zhang and W. Zhang, "Linear active disturbance rejection control and parameter tuning of magnetic levitation ball system," *Syst. Sci. Math.*, vol. 37, no. 8, pp. 1741–1756, 2017.
[33] Y. Sun, H. Qiang, L. Wang, W. Ji, and A. Mardani, "A fuzzy-logic system-based cooperative control for the multi-electromagnets suspension system of maglev trains with experimental verification," *IEEE Trans. Fuzzy Syst.*, early access, Mar. 14, 2023, doi: 10.1109/TFUZZ.2023.3257036.

YUNPENG JU received the M.S. degree in control theory and control engineering and the Ph.D. degree in mechanical design and theory from the Qingdao University of Science and Technology, Qingdao, China, in 2013 and 2016, respectively. He is currently a master's supervisor. His current research interests include mechanical dynamics, robot control and navigation, modeling, and control of complex nonlinear systems.

YALIN ZHANG received the B.S. degree in automation from the Qingdao University of Science and Technology, Qingdao, China, in 2021, where he is currently pursuing the M.S. degree in control engineering. His current research interests include linear active disturbance rejection control and quadrotor unmanned aerial vehicles.

GUIXIN ZHU received the B.S. degree in mechatronics from Southeast University, Nanjing, China, in 1997, and the M.S. degree in control engineering from the Qingdao University of Science and Technology, Qingdao, China, in 2009. He is currently with the Qingdao University of Science and Technology. His current research interests include mechanical dynamics, robot control, and navigation.